

Study of the reverse saturation current and series resistance of p-p-n perovskite solar cells using the single and double-diode models

M.A. Cappelletti^{a,b,c,*}, G.A. Casas^{c,d}, A.P. Cédola^{c,e}, E.L. Peltzer y Blanca^{a,c}, B. Marí Soucase^f

^a Comisión Nacional de Investigaciones Científicas (CONICET), Argentina

^b Universidad Nacional Arturo Jauretche (UNAJ), Avenida Calchaquí 6200, Florencio Varela, 1888, Buenos Aires, , Argentina

^c Grupo de Estudio de Materiales y Dispositivos Electrónicos (GEMyDE), Dpto. Electrotecnia, Facultad de Ingeniería, Universidad Nacional de La Plata, Calle 48 y 116, La Plata, 1900, Buenos Aires, Argentina

^d Universidad Nacional de Quilmes, Roque Saenz Peña 352, Bernal, 1876, Buenos Aires, Argentina

^e Comisión de Investigaciones Científicas, Provincia de Buenos Aires (CIC), Argentina

^f Departament de Física Aplicada-ETSED, Universitat Politècnica de València, Camí de Vera s/n, València, 46022, Spain

ARTICLE INFO

Keywords:

Perovskite solar cells
Hole Transporting Material (HTM)
One and two-diode models
Genetic algorithm
Parameters extraction

ABSTRACT

The effects of the offset level and of the doping level in the perovskite layer upon both the reverse saturation current (J_0) and the series resistance (R_s) of p-p-n perovskite solar cells have been researched in this paper, using five different materials such as spiro-OMeTAD, Cu₂O, CuSCN, NiO and CuI, as Hole Transporting Material (HTM). The analysis was carried out by means of the single and double-diode models of a solar cell and of genetic algorithms based on optimization technique, in order to extract the desired parameters. The minor degradation of J_0 and R_s has been found for the condition offset equal to zero and for the highest doping level in p-type perovskite layer. Also, a comparison has been made of the behavior of two reverse saturation currents (J_{01} and J_{02}). The power conversion efficiency (PCE) has shown to be more strongly dependent on J_{02} than on J_{01} . Results obtained in this work can be used to improve the manufacturing process of these devices.

1. Introduction

Energy is a strategic resource for the development of any country. The continuous increase in energy demand together with the associated environmental impact of fossil fuel combustion is strong incentives to promote the study and development of new technologies based on renewable energies such as photovoltaic (PV) and wind power generation systems. Solar energy is the most promising renewable energy source to generate electric power and to reduce the carbon dioxide (CO₂) emissions to the atmosphere.

The study of materials and their microscopic properties together with the development of advanced device fabrication processes has opened the way to new research possibilities in photovoltaic technology in order to improve the performance of the PV cells.

In the last years, research on perovskite solar cells has attracted the interest of the scientific community due to its high power conversion efficiency (PCE) at low cost [1–6]. Experimental studies of the perovskite solar cells have reported a significant increase in PCE, from 3.8% in 2009 [7] to 22.7% recently [8], confirming the upward trend of this promising technology. Moreover, these

* Corresponding author. Universidad Nacional Arturo Jauretche (UNAJ), Avenida Calchaquí 6200, Florencio Varela, 1888, Buenos Aires, Argentina.

E-mail address: mcappelletti@unaj.edu.ar (M.A. Cappelletti).

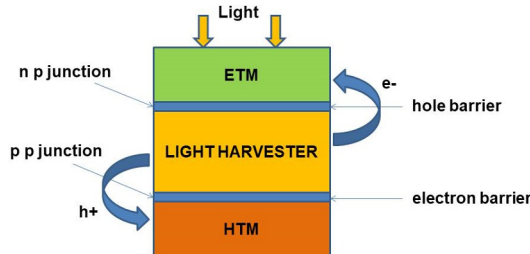


Fig. 1. The planar structure of a perovskite solar cell.

devices can be used to generate a solar-to-hydrogen conversion in water photolysis applications [9]. Therefore, further experimental and theoretical studies are required in order to have a better understanding of the behavior of perovskite solar cells and to optimize the design of the structure and the selection of materials.

A typical planar structure of perovskite solar cells composed of three regions: HTM/Perovskite/ETM is shown in Fig. 1, where HTM and ETM are the p-type hole-transporting material and the n-type electron-transporting material, respectively. The solar energy is absorbed by the p-type central material called perovskite layer, where after the charge carriers are photogenerated and extracted towards the electrodes, by transporting holes and electrons through the HTM and ETM layers, respectively.

A comparative theoretical study of perovskite solar cells of structure HTM/CH₃NH₃PbI₃/TiO₂ has been recently developed by the authors through computer simulation using an organic compound (spiro OMeTAD) and four different inorganic materials (Cu₂O, CuSCN, NiO and CuI) as HTM layer [10]. These inorganic compounds are promising candidates to replace the less stable and more expensive organic compound spiro-OMeTAD (2,2',7,7'-tetrakis (N,N-di-p-methoxyphenylamine)-9,9'-spirobifluorene). The five materials considered as HTM layer have different band gap energies (E_g) and electron affinities (X_e), which leads to different alignments between the Maximum of the Valence Band (MVB) of both the HTM and the perovskite layers, which is referred as the offset level ($\text{Offset} = \text{MVB}_{\text{HTM}} - \text{MVB}_{\text{Perovskite}}$). The results obtained in Ref. [10] have shown a strong dependence of PCE with both the offset level and the doping level in p-type perovskite layer. Also, since Cu₂O is the material with the lowest offset level (0.06 eV), the highest value of PCE has been obtained for the Cu₂O/CH₃NH₃PbI₃/TiO₂ solar cell.

For a better and more detailed understanding of the behavior of the perovskite solar cells, new studies on the same group of devices analyzed in Ref. [10] are presented here. Specifically, in this work, the effects of the offset level and of the doping level in the perovskite layer upon both the reverse saturation currents and the series resistance of these devices have been researched by means of the single and double-diode models of a solar cell and of a home-made numerical code based on genetic algorithms. The authors have previously used genetic algorithms based on optimization technique in order to extract the parameters of GaAs sub-cells for triple junction space solar cells [11].

The study of the reverse saturation currents is very useful to determine which conduction mechanism is predominant: the diffusion or the recombination process. It is possible to use the single or double-diode models for extraction of perovskite solar cell parameters since the planar-structured solar cells can in general be treated as a single p-n junction diode [12]. Different planar perovskite solar cells have been studied in Ref. [12] using the single-diode model.

2. Material and methods

2.1. Extraction of solar cells parameters

The current-voltage output characteristic ($J-V$) of solar cells provides information about different parameters of interest of the devices, such as photocurrent, reverse saturation current, ideality factor, series resistance and shunt resistance. Having an accurate

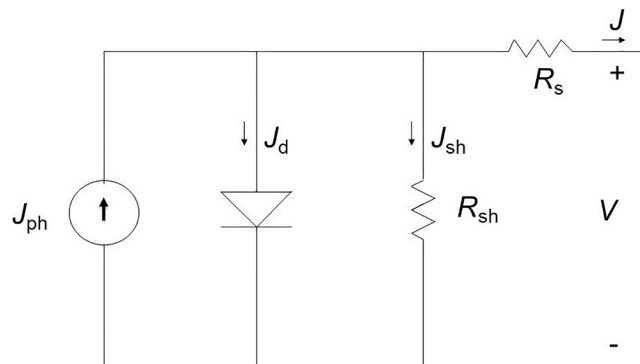


Fig. 2. Equivalent circuit model of a solar cell: (a) The one-diode model, and (b) The two-diode model.

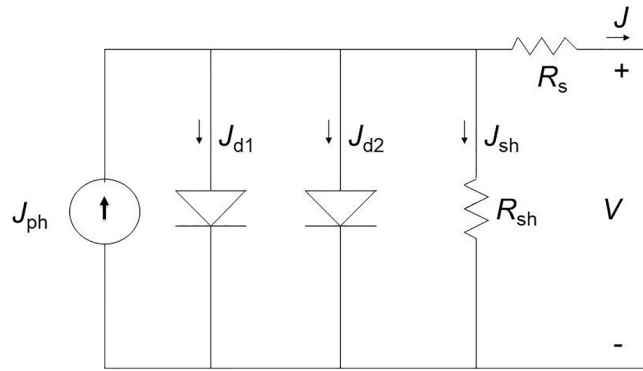


Fig. 2. (continued)

knowledge of these parameters is essential for evaluating the performance of the solar cells, for optimizing devices structure, for improving the fabrication process as well as in devices modelling and simulation [13,14]. These parameters can be accurately extracted from equations corresponding to the single or double diode models, which are the two main equivalent circuit models widely used to describe the nonlinear I–V behavior of a solar cell with or without illumination. These models are basically derived from the semiconductor equations that govern the physics of solar cells [15].

In the first case, one diode is connected in parallel to a light generated current source (J_{ph}), such as is shown in Fig. 2(a), where J_d and J_{sh} are the current densities through the diode and the shunt resistance, respectively. The series resistance R_s represents the ohmic losses in the semiconductor bulk and in the metallic contacts, whereas the shunt resistance R_{sh} represents the current leakages across the p-n junction. Finally, J and V are the output current and the output voltage of the solar cell respectively, which are related through the following equation [16]:

$$J(V) = J_{ph} - J_d - J_{sh} = J_{ph} - J_0 \left\{ \exp \left[\frac{q(V + JR_s)}{nkT} \right] - 1 \right\} - \frac{V + JR_s}{R_{sh}} \quad (1)$$

where J_0 is the reverse saturation current of diode, n is the diode ideality factor, q is the electronic charge, k is the Boltzmann's constant and T is the temperature in kelvin.

On the other hand, Fig. 2(b) shows the double diode equivalent circuit model, where two diodes are connected in parallel to the current source and therefore a new current component with an exponential term is added to equation (1). This model allows to obtain a better understanding of the physical phenomena within the device, since it can be used to study the space charge recombination effect. The current J_{d1} represent the diffusion mechanism, including the recombination and drift occurring in the bulk material; and the current J_{d2} corresponds to the carrier recombination and generation in the space-charge region of the junction and to surface recombination [17]. The R_s and R_{sh} are similar to those corresponding to the one-diode model. In this case, the output current J and the output voltage V are related by Ref. [18]:

$$\begin{aligned} J(V) = J_{ph} - J_{d1} - J_{d2} - J_{sh} &= J_{ph} - J_{01} \left\{ \exp \left[\frac{q(V + JR_s)}{n_1 kT} \right] - 1 \right\} \\ &\quad - J_{02} \left\{ \exp \left[\frac{q(V + JR_s)}{n_2 kT} \right] - 1 \right\} - \frac{V + JR_s}{R_{sh}} \end{aligned} \quad (2)$$

where J_{01} and J_{02} are the reverse saturation currents of diodes 1 and 2, respectively. Also, n_1 and n_2 are the diode ideality factors, respectively.

From equations (1) and (2), it can be seen that for modelling the I–V characteristics of a solar cell, it is necessary to extract five (J_{ph} , J_0 , R_s , R_{sh} , n) and seven (J_{ph} , J_{01} , J_{02} , R_s , R_{sh} , n_1 , n_2) parameters, respectively. These equations describe the performance of a solar cell under illumination or in dark conditions. However, they are transcendental equations that cannot be solved algebraically. Hence, the use of optimization methods to extract the unknown parameters are required.

Many parameters extraction techniques using equations (1) and (2) have been proposed in the literature, such as the Newton–Raphson Method (NRM) and the Levenberg–Marquardt Algorithm (LMA), which are both based on the gradient descent approach [19]. In recent years, heuristic methods such as genetic algorithms, have been used to improve the accuracy and computational efficiency for extraction of solar cell parameters as compared to conventional techniques, due to their known advantages related to the global minimum finding, easy of coding, etc. [11,20,21]. The genetic algorithms method, inspired by the biological evolution process, is based on the global search and optimization techniques [22]. This method does not determine a unique solution since there may be more than one combination of input parameters that yields the same output value. However, it is a powerful tool for obtaining approximate solutions to the exact solutions.

2.2. Simulation details

With the aim to understanding the behavior of different p-p-n perovskite solar cells, a numerical code based on genetic algorithms, fully developed by the authors in Python, has been used in order to extract the reverse saturation current, the series resistance

Table 1
Characteristic parameters of the twelve solar cells under study.

Solar Cell	HTM	Offset (eV)	N_A (cm^{-3})
SC_1	Cu ₂ O	0.06	10^{17}
SC_2	CuSCN	0.13	10^{17}
SC_3	NiO	0.17	10^{17}
SC_4	CuI	0.23	10^{17}
SC_5	spiro-OMeTAD	0.32	10^{17}
SC_6	Cu ₂ O	0	10^{17}
SC_7	Cu ₂ O	0.16	10^{17}
SC_8	Cu ₂ O	0.26	10^{17}
SC_9	Cu ₂ O	0.36	10^{17}
SC_10	Cu ₂ O	0.06	10^{18}
SC_11	Cu ₂ O	0.06	10^{19}
SC_12	Cu ₂ O	0.06	10^{20}

and the ideality factor from equations (1) and (2). In particular, twelve devices of planar structure HTM/CH₃NH₃PbI₃/TiO₂ have been analyzed, which are similar to those studied in Ref. [10], where HTM is one of the following materials: Cu₂O, CuSCN, NiO, CuI and spiro-OMeTAD. Table 1 displays the complete set of the solar cells researched in this work, where the offset level is defined as $\text{Offset} = MVB_{\text{HTM}} - MVB_{\text{Perovskite}}$; and N_A is the acceptor carrier concentration in the perovskite layer. It is considered that the solar radiation enter through the n-type transparent conducting oxide TiO₂. The standard AM1.5G spectrum (1000 Wm⁻²; T = 300 K) has been used.

Table 2 summarizes the main physical parameters used for each layer in the one-dimensional code SCAPS-1D (Solar Cells Capacitance Simulator) [23] in order to obtain the I–V characteristic of the solar cells described in Table 1, where E_g is the band gap energy, X_e is the electron affinity, N_C and N_V are the effective density of states (DOS) in the conduction and the valence bands, respectively; μ_n and μ_p are the electron and hole mobilities, respectively; ϵ is the relative permittivity; and N_A and N_D are the acceptor and donor carrier concentrations, respectively. These values are similar to those used by authors in Ref. [10].

The genetic algorithm based on optimization technique used in this work was implemented according to the following considerations:

- Binary representation is used as a solution encoding.

Table 2
Main physical parameters used for each layer in the SCAPS-1D software.

	Cu ₂ O	CuSCN	NiO	CuI	spiro-OMeTAD
HTM (400 nm)	E_g (eV) X_e (eV) N_C (cm^{-3}) N_V (cm^{-3}) μ_n ($\text{cm}^2\text{V}^{-1}\text{s}^{-1}$) μ_p ($\text{cm}^2\text{V}^{-1}\text{s}^{-1}$) ϵ N_A (cm^{-3}) N_D (cm^{-3})	2.17 3.2 2.50×10^{20} 2.50×10^{20} 80 80 6.6 3.00×10^{18} 0	3.6 1.7 2.50×10^{20} 2.50×10^{20} 25 25 5.1 3.00×10^{18} 0	3.8 1.46 2.50×10^{20} 2.50×10^{20} 2.8 2.8 11.7 3.00×10^{18} 0	3.1 2.1 2.50×10^{20} 2.50×10^{20} 44 44 6.5 3.00×10^{18} 0
Perovskite (400 nm)	E_g (eV) X_e (eV) N_C (cm^{-3}) N_V (cm^{-3}) μ_n ($\text{cm}^2\text{V}^{-1}\text{s}^{-1}$) μ_p ($\text{cm}^2\text{V}^{-1}\text{s}^{-1}$) ϵ N_A (cm^{-3}) N_D (cm^{-3})	1.5 3.93 2.50×10^{20} 2.50×10^{20} 50 50 30 1.00×10^{17} 0			
TiO ₂ (90 nm)	E_g (eV) X_e (eV) N_C (cm^{-3}) N_V (cm^{-3}) μ_n ($\text{cm}^2\text{V}^{-1}\text{s}^{-1}$) μ_p ($\text{cm}^2\text{V}^{-1}\text{s}^{-1}$) ϵ N_A (cm^{-3}) N_D (cm^{-3})	3.26 4.2 1.00×10^{21} 2.00×10^{20} 1.00×10^{-3} 1.00×10^{-3} 100 5.00×10^{18} 5.00×10^{19}			

- The fitness function is based on equations (1) and (2), expressed as:

$$\begin{aligned} f(J_{\text{ph}}, J_0, R_s, R_{\text{sh}}, n) &= J_{\text{ph}} - J - J_d - J_{\text{sh}} \\ &= J_{\text{ph}} - J - J_0 \left\{ \exp \left[\frac{q(V+JR_s)}{nkT} \right] - 1 \right\} - \frac{V+JR_s}{R_{\text{sh}}} \end{aligned} \quad (3)$$

and

$$\begin{aligned} f(J_{\text{ph}}, J_{01}, J_{02}, R_s, R_{\text{sh}}, n_1, n_2) &= J_{\text{ph}} - J - J_{d1} - J_{d2} - J_{\text{sh}} \\ &= J_{\text{ph}} - J - J_{01} \left\{ \exp \left[\frac{q(V+JR_s)}{n_1 kT} \right] - 1 \right\} \\ &\quad - J_{02} \left\{ \exp \left[\frac{q(V+JR_s)}{n_2 kT} \right] - 1 \right\} - \frac{V+JR_s}{R_{\text{sh}}} \end{aligned} \quad (4)$$

respectively.

- Random selection of the initial population.
- Initial population size: 500 individuals.
- Roulette wheel is used as method of selecting individuals for reproduction.
- The one-point crossover is employed with the crossover probability 0.7.
- Mutation probability 0.005.
- The genetic algorithm is executed 1000 generations.

The input data for the genetic algorithm are a set of $N = 50$ values taken from each J - V curve. The optimum solution is achieved when the fitness function is $f(\dots) = 0$ for any J - V pair. The Root Mean Square Error ($RMSE$) is used in order to evaluate the performance of the technique based on genetic algorithms, which is calculated as:

$$RMSE = \sqrt{\frac{1}{N} \sum_{i=1}^N f_i(\dots)^2} \quad (5)$$

3. Results and discussion

3.1. Analysis with the one-diode model of a solar cell

Five parameters, such as J_{ph} , J_0 , R_s , R_{sh} and n , can be extracted from the single diode model of a solar cell. It is often assumed that the light generated current density, J_{ph} , to be equal to the short-circuit current density J_{sc} [19]. Additionally, the effect of R_{sh} can be negligible. Thus, the solar cell parameter extraction problem reduces to the determination of three parameters: J_0 , R_s and n , from the J - V characteristics. An efficient solar cell structure would possess low values in both parameters: J_0 and R_s .

The results obtained of the extraction of J_0 and R_s using genetic algorithms (GA) for the complete set of the solar cells studied in this work are summarized in the second and third column of Table 3, respectively. An optimum value of n equal to 1.44 has been extracted and fixed in all cases. The fourth column presents the $RMSE$ values calculated with equation (5). Table 3 also presents the values of short-circuit current density J_{sc} , open circuit voltage V_{oc} and power conversion efficiency PCE , which were obtained from the SCAPS-1D software.

As can be observed in Table 3 the values of V_{oc} and PCE suffer significant variations with respect to both the offset level and the acceptor carrier concentration in the perovskite layer, whereas no changes were obtained in the values of J_{sc} for all devices considered here. Therefore, for the purpose of a better understanding of this behavior, an analysis of the data of J_0 and R_s taken from

Table 3

Parameters extraction results of the solar cells described in Table 1 using the one-diode model.

Solar Cell	J_0 (Acm $^{-2}$) (GA)	R_s (Ω) (GA)	$RMSE$ (Acm $^{-2}$) (GA)	J_{sc} (mA cm $^{-2}$) (SCAPS-1D)	V_{oc} (V) (SCAPS-1D)	PCE (%) (SCAPS-1D)
SC_1	4.64×10^{-17}	0.34	1.93×10^{-3}	23.64	1.22	25.06
SC_2	1.18×10^{-16}	0.46	4.42×10^{-4}	23.65	1.21	24.86
SC_3	2.31×10^{-16}	0.59	1.28×10^{-3}	23.65	1.21	24.57
SC_4	7.21×10^{-16}	0.81	3.47×10^{-3}	23.65	1.19	23.78
SC_5	4.46×10^{-15}	1.35	4.49×10^{-3}	23.65	1.12	21.79
SC_6	2.35×10^{-17}	0.31	2.35×10^{-3}	23.64	1.23	25.10
SC_7	1.85×10^{-16}	0.56	2.51×10^{-4}	23.64	1.21	24.44
SC_8	1.22×10^{-15}	0.97	3.77×10^{-3}	23.65	1.17	23.09
SC_9	2.01×10^{-14}	1.63	1.03×10^{-3}	23.65	1.09	20.99
SC_10	9.20×10^{-18}	0.22	2.11×10^{-3}	23.64	1.23	25.62
SC_11	4.42×10^{-18}	0.15	1.32×10^{-3}	23.65	1.26	26.64
SC_12	2.59×10^{-18}	0.12	1.30×10^{-3}	23.67	1.30	27.44

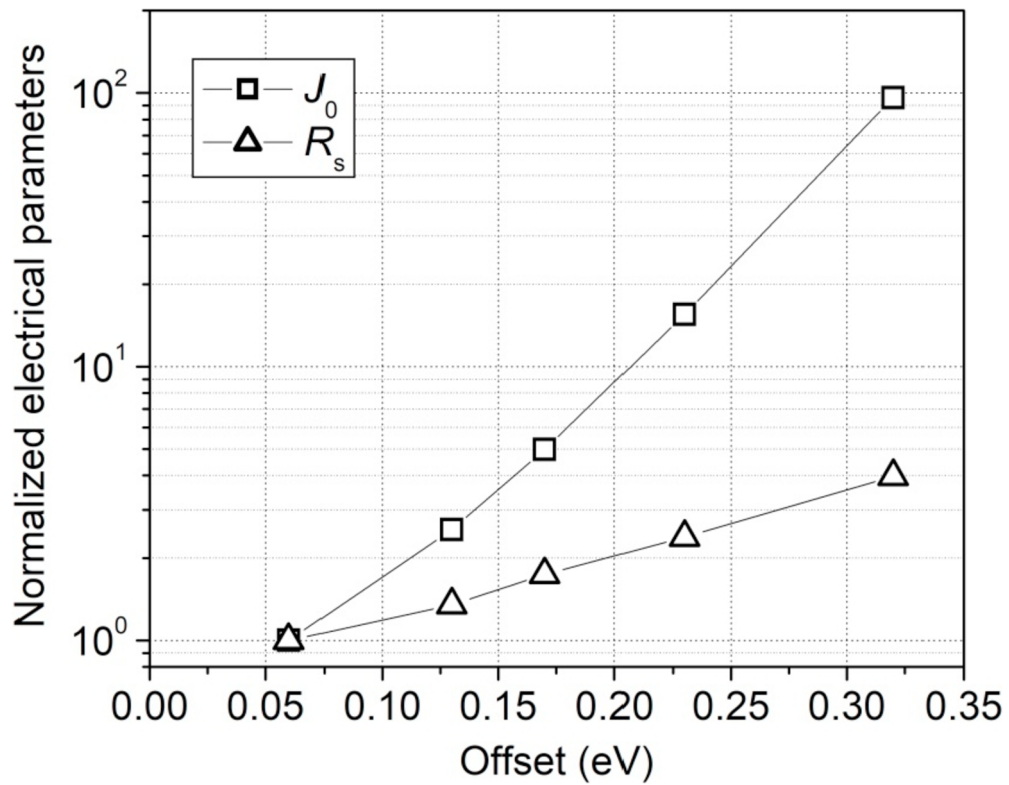


Fig. 3. Normalized electrical parameters as a function of the offset level for the five different HTM materials considered in this work.

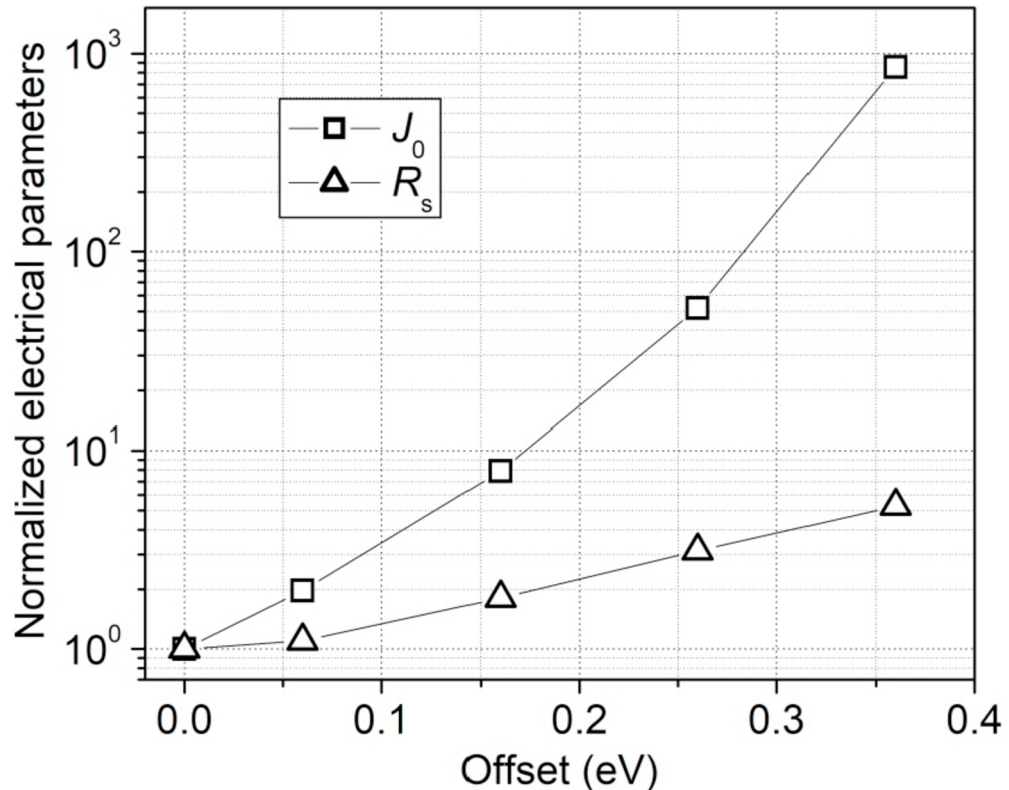


Fig. 4. Normalized electrical parameters as a function of the offset level for the $\text{Cu}_2\text{O}/\text{Perovskite}/\text{TiO}_2$ solar cell.

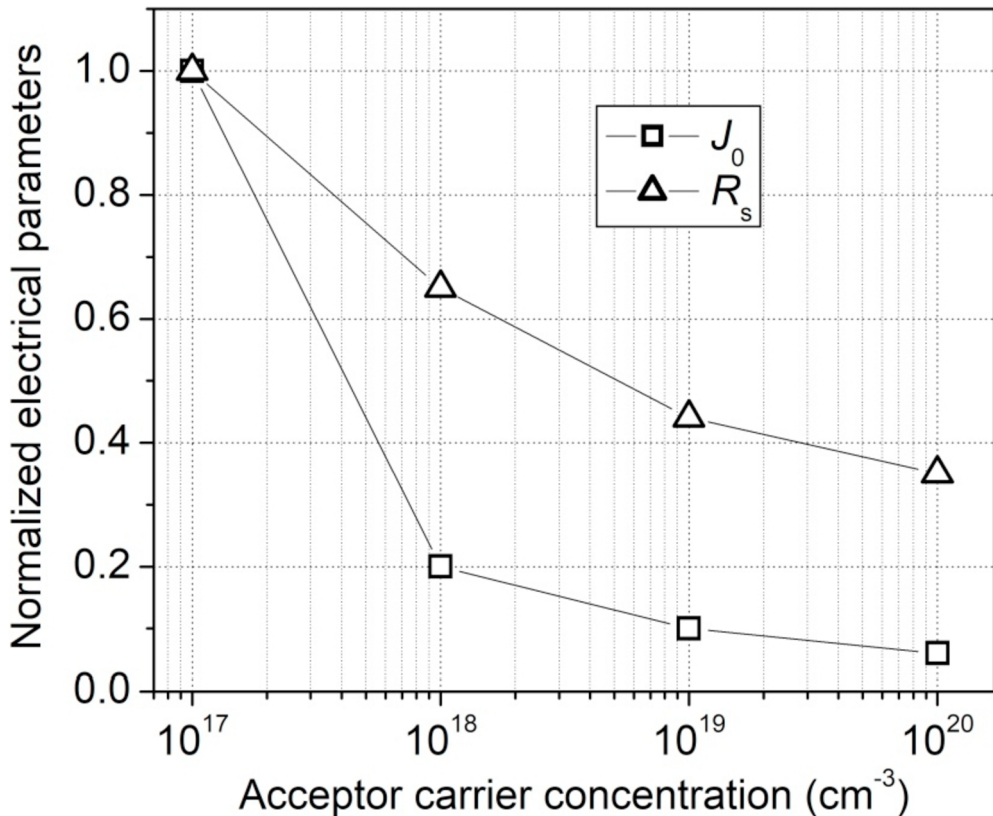


Fig. 5. Normalized electrical parameters as a function of the acceptor carrier concentration in the perovskite layer for the $\text{Cu}_2\text{O}/\text{Perovskite}/\text{TiO}_2$ solar cell.

Table 4

Parameters extraction results of the solar cells described in Table 1 using the two-diode model.

Solar Cell	J_{01} (Acm^{-2})	J_{02} (Acm^{-2})	RMSE (Acm^{-2})	PCE (%)
SC_1	6.81×10^{-17}	1.91×10^{-12}	1.41×10^{-3}	25.06
SC_2	1.02×10^{-16}	1.70×10^{-11}	3.93×10^{-4}	24.86
SC_3	1.43×10^{-16}	3.52×10^{-11}	2.24×10^{-4}	24.57
SC_4	2.30×10^{-16}	9.38×10^{-11}	6.84×10^{-4}	23.78
SC_5	8.14×10^{-16}	3.50×10^{-10}	3.84×10^{-4}	21.79
SC_6	5.54×10^{-17}	1.49×10^{-13}	1.66×10^{-3}	25.10
SC_7	1.28×10^{-16}	2.88×10^{-11}	1.21×10^{-4}	24.44
SC_8	3.06×10^{-16}	1.55×10^{-10}	7.47×10^{-4}	23.09
SC_9	2.04×10^{-15}	4.98×10^{-10}	4.73×10^{-4}	20.99
SC_10	4.30×10^{-17}	1.07×10^{-14}	1.43×10^{-3}	25.62
SC_11	3.04×10^{-17}	1.04×10^{-15}	3.98×10^{-4}	26.64
SC_12	1.44×10^{-17}	2.68×10^{-16}	1.93×10^{-4}	27.44

Table 3 are shown in Fig. 3, Fig. 4 and Fig. 5. The lines through the data points are only intended to guide the eye.

Fig. 3 shows the variation of J_0 and R_s parameters with respect to the offset level of the five different materials considered for the HTM layer (SC_1, SC_2, SC_3, SC_4 and SC_5). The values presented are normalized to those corresponding to the offset level equal to 0.06 eV (i.e. Cu_2O as HTM layer), which are $4.64 \times 10^{-17} \text{ Acm}^{-2}$ and 0.34Ω , for J_0 and R_s , respectively. This figure shows that J_0 and R_s reach the lowest values for the $\text{Cu}_2\text{O}/\text{CH}_3\text{NH}_3\text{PbI}_3/\text{TiO}_2$ heterojunction as compared to the corresponding parameters of the devices based on the other four hole-transport materials. It can also be seen an abrupt increase in J_0 (close to 2 orders of magnitude) and a gradual increase of R_s (close to 4 times) when the offset level is increased. These significant increases in J_0 and R_s could explain the reduction of the PCE, from 25.06% to 21.79% for Cu_2O and spiro-OMeTAD, respectively.

Since the Cu_2O is the material with the lowest real offset (0.06 eV), Figs. 4 and 5 show the results obtained of the extraction of electrical parameters on the $\text{Cu}_2\text{O}/\text{CH}_3\text{NH}_3\text{PbI}_3/\text{TiO}_2$ solar cells. Specifically, Fig. 4 shows the normalized data (J_0 and R_s) as a function of the offset level (SC_1, SC_6, SC_7, SC_8 and SC_9). The offset level was artificially modified by changing the electron affinity of Cu_2O . In this case, the values presented are normalized to those corresponding to the offset level equal to zero, which are

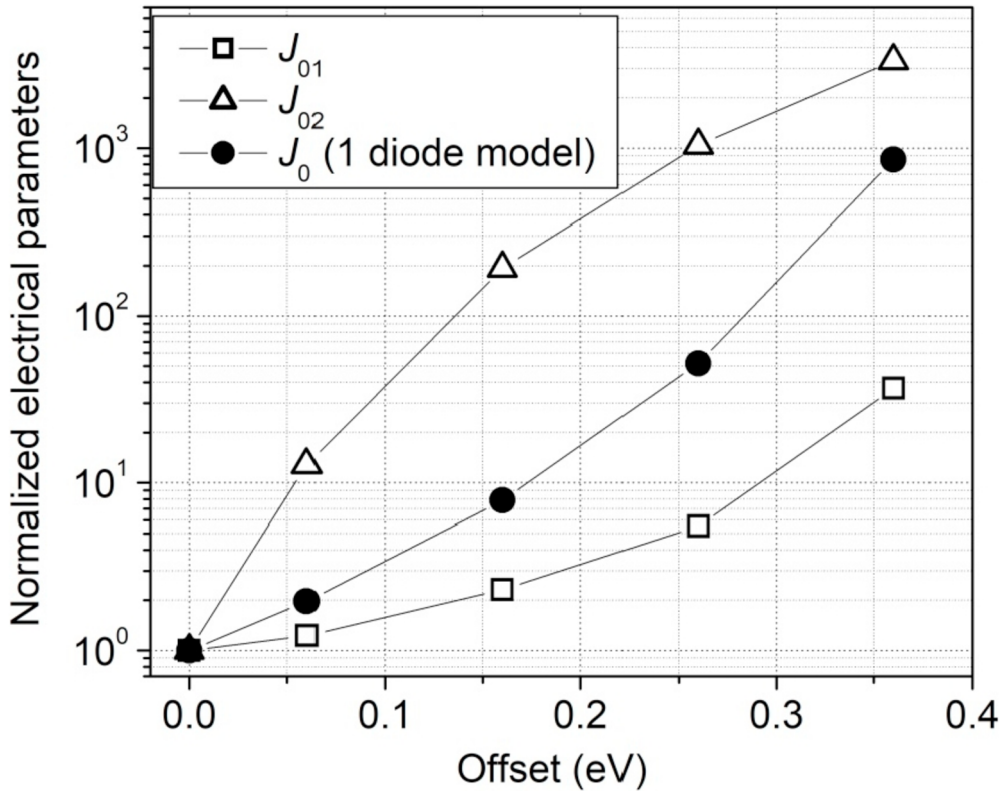


Fig. 6. Normalized electrical parameters as a function of the offset level for the Cu₂O/Perovskite/TiO₂ solar cell.

2.35×10^{-17} Acm⁻² and 0.31Ω , for J_0 and R_s , respectively. The data set presented in Fig. 4 show a similar behavior to that described in Fig. 3. It can also be observed that the best condition to achieve the lesser degradation in J_0 and R_s is obtained for when the offset level is equal to zero. Under this condition, no differences in the value of PCE were found using CuSCN, CuI and NiO as HTM layer, whereas for spiro-OMeTAD the value of PCE is reduced due to its very low value of hole mobility [10].

Finally, effects of the acceptor carrier concentration in the perovskite layer upon the J_0 and R_s values are shown in Fig. 5 for the condition offset equal to 0.06 eV (SC_1, SC_10, SC_11 and SC_12). These values are presented as normalized with respect to those corresponding to the N_A equal to 10^{17} cm⁻³, which are 4.64×10^{-17} Acm⁻² and 0.34Ω , for J_0 and R_s , respectively. It is possible to observe in this figure that when N_A is increased from 10^{17} to 10^{20} cm⁻³, then J_0 and R_s decrease about 95% and 65%, respectively. Therefore, the decreasing of J_0 and R_s could be the main reason for the increase of PCE from 25.06% to 27.44%.

3.2. Analysis with the two-diode model of a solar cell

The addition of a second diode to the previous model, makes it possible to study in more detail the space charge recombination effect. The second diode in the double-diode model contributes two additional parameters: the reverse saturation current J_{02} and the ideality factor n_2 . Therefore, from this model seven parameters can be extracted, J_{ph} , J_{01} , J_{02} , R_s , R_{sh} , n_1 and n_2 . In a similar way to the analysis carried out previously with the single-diode model, it was assumed that $J_{ph} = J_{sc}$ and the effect of R_{sh} was considered negligible. Also, the R_s parameter was taken with the values presented in Table 3. Thus, in this case, from the J-V curves, the solar cell parameter extraction problem reduces to determination of four parameters: J_{01} , J_{02} , n_1 and n_2 .

Table 4 contains the results obtained using genetic algorithms of the extraction of J_{01} and J_{02} for the twelve solar cells studied in this work. The optimum values of n_1 equal to 1.44 and of n_2 equal to 2.50 have also been extracted and fixed in all cases. Ideality factors higher than 2 have also been obtained for different perovskite solar cells in Ref. [12]. The fourth column presents the RMSE values calculated with equation (5). Finally, for convenience, in Table 4 the values of PCE are also shown.

The values obtained for J_{01} and J_{02} in Table 4 are consistent with literature data since J_{02} is generally 3 to 7 orders of magnitude larger than J_{01} [18]. An analysis of the data of J_{01} and J_{02} taken from Table 4 are shown in Fig. 6 and Fig. 7.

Fig. 6 shows data of J_{01} and J_{02} as a function of the offset level on the Cu₂O/CH₃NH₃PbI₃/TiO₂ solar cells (SC_1, SC_6, SC_7, SC_8 and SC_9). These values are normalized to those corresponding to the offset level equal to zero (SC_6), which are 5.54×10^{-17} Acm⁻² and 1.49×10^{-13} Acm⁻², for J_{01} and J_{02} , respectively. As a comparison, it has also been added in Fig. 6 the data of J_0 shown previously in Fig. 4. It can be seen in Fig. 6 a much greater increase in J_{02} (close to 3300 times) than in J_{01} (close to 37 times), when the offset level is increased from 0 to 0.36 eV. Therefore, the decrease in PCE, from 25.10% to 20.99% is a major consequence of the

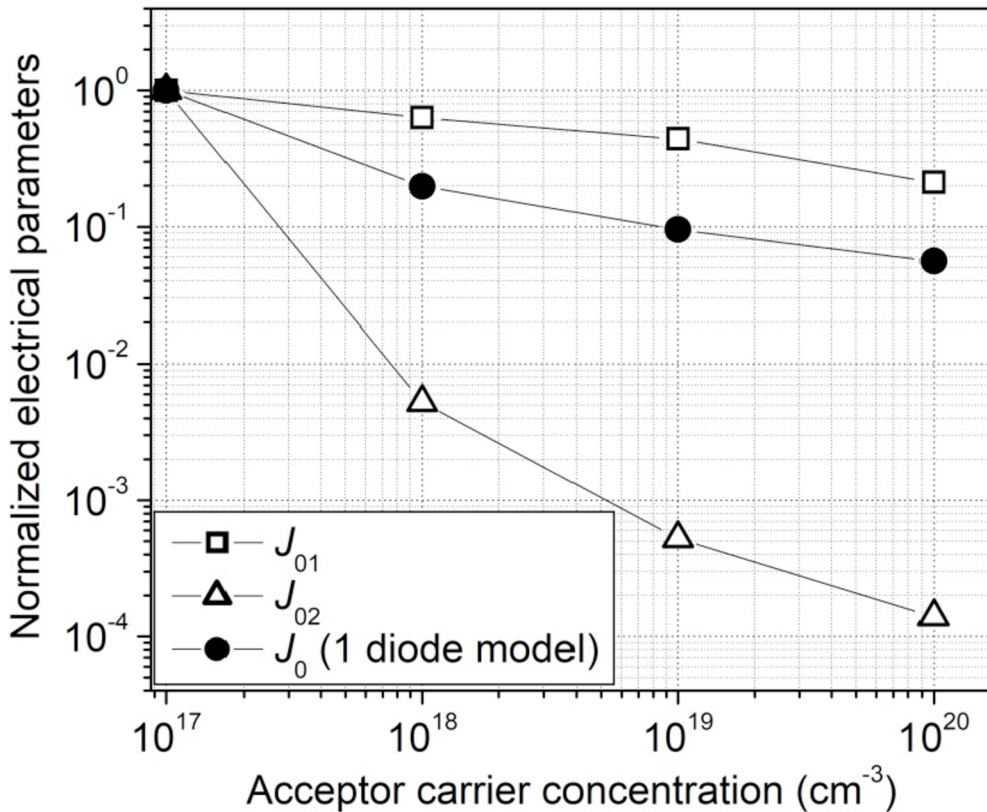


Fig. 7. Normalized electrical parameters as a function of the acceptor carrier concentration in the perovskite layer for the $\text{Cu}_2\text{O}/\text{Perovskite}/\text{TiO}_2$ solar cell.

strong increase in the carrier recombination in the space-charge region of the junction.

Fig. 7 shows the normalized data for J_{01} and J_{02} , calculated by varying the acceptor carrier concentration in the perovskite layer (SC_1, SC_10, SC_11 and SC_12). The values presented are normalized to those corresponding to the N_A equal to 10^{17} cm^{-3} , which are $J_{01} = 6.81 \times 10^{-17} \text{ Acm}^{-2}$ and $J_{02} = 1.91 \times 10^{-12} \text{ Acm}^{-2}$. Again, as a comparison, it has also been added in Fig. 7 the data of J_0 shown previously in Fig. 5. In this case, it can be observed that when N_A is increased from 10^{17} to 10^{20} cm^{-3} , then J_{02} decreases more strongly (close to 4 orders of magnitude) than J_{01} (about 80%), which tend to improve the solar cell performance.

In order to better understand the physical mechanisms of conduction present within the devices, we have plotted in Fig. 8 the variation of the current components through the two diodes, J_{d1} and J_{d2} , calculated as:

$$J_{d1,d2} = J_{01,02} \left\{ \exp \left[\frac{q(V + JR_s)}{n_{1,2}kT} \right] - 1 \right\} \quad (6)$$

as a function of the voltage, for the two extreme cases: devices with the minimum and the maximum PCE values (SC_9 and SC_12, respectively).

Fig. 8 shows that for the SC_9 device ($PCE = 20.99\%$), the dominant effect from 0 V to V_{oc} is the minority carrier recombination in the space-charge region. On the contrary, for the SC_12 device ($PCE = 27.44\%$), two different behaviors occur within the device. At voltages below 0.25 V, the effect of J_{d2} is more significant than J_{d1} , whereas the current flow controlled by minority carrier diffusion outside the space-charge region is the dominant effect at voltages from 0.25 V to V_{oc} . For all solar cells considered in this work, the values of the slopes are $\frac{q}{n_1 kT}$ and $\frac{q}{n_2 kT}$ for J_{d1} and J_{d2} , respectively. Besides, it has been found that as the value of PCE increases from 20.99% to 27.44%, the value of voltage for which both mechanisms have the same effect ($J_{d1} = J_{d2}$) decreases from 1.09 V to 0.25 V.

4. Conclusion

The results obtained in this work have allowed us to study in detail the physical mechanisms of conduction present within the perovskite solar cells and are useful to contribute to the design, optimization and manufacturing process of such devices. This paper continues the research started in a recent work of the authors. In the study performed here, the behavior of the reverse saturation current and the series resistance of perovskite solar cells of structure $\text{HTM}/\text{CH}_3\text{NH}_3\text{PbI}_3/\text{TiO}_2$ with five different Hole Transporting Material (HTM), such as spiro-OMeTAD, Cu_2O , CuSCN , NiO and CuI , has been discussed. These parameters have been extracted using genetic algorithms based on optimization technique and the single and double-diode models of a solar cell. It has been observed that

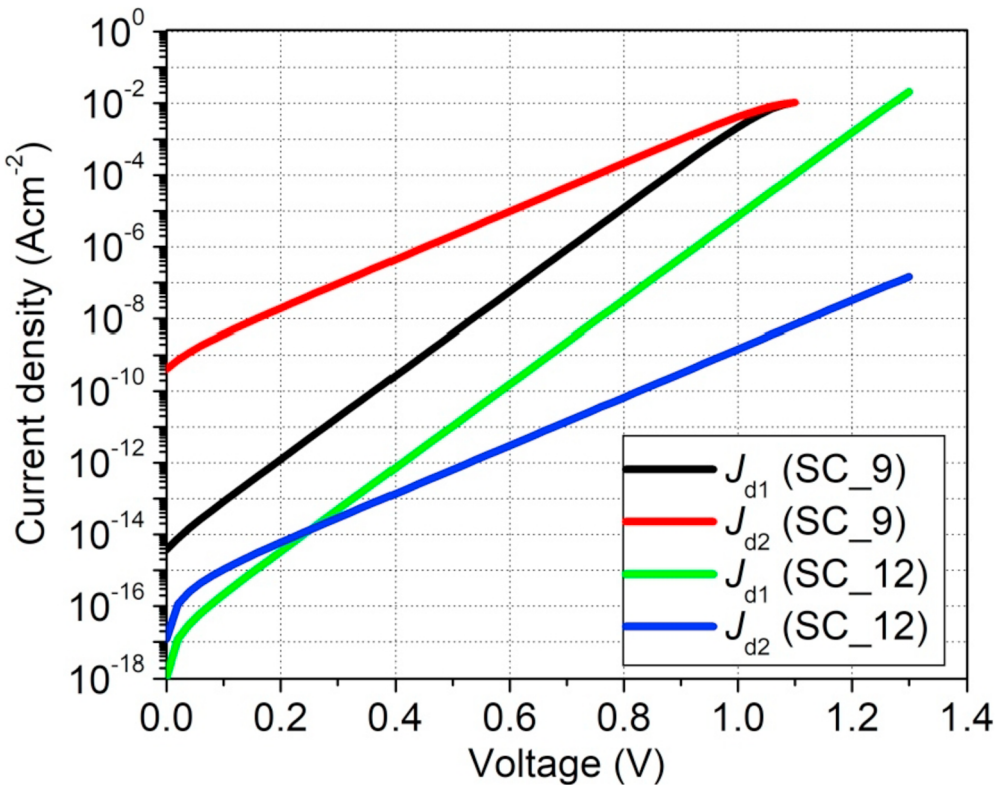


Fig. 8. Current density components-Voltage curves for two $\text{Cu}_2\text{O}/\text{Perovskite}/\text{TiO}_2$ solar cells, with the minimum and maximum values of PCE.

these parameters are strongly dependent on both the alignment between the Maximum of the Valence Band (MVB) of the HTM and perovskite layers (offset level), and the doping level in p-type perovskite layer. Specifically, it has been obtained that the increase in the offset level from 0 to 0.36 eV, produces an abrupt increase in J_0 (close to 3 orders of magnitude) and a gradual increase of R_s (close to 5 times), which could explain the reduction of the PCE from 25.10% to 20.99%. In opposition, J_0 and R_s decrease about 95% and 65%, respectively in the case that the acceptor carrier concentration in the perovskite layer has gone increasing from 10^{17} to 10^{20} cm^{-3} , which could be the main reason for the increase of PCE from 25.06% to 27.44%. Besides, a comparison has been made of the behavior of two reverse saturation currents (J_{01} and J_{02}). It has been found that the offset level and of the doping level in the perovskite layer affect more strongly to J_{02} than J_{01} . Finally, it has also been found that when the carrier recombination and generation mechanisms in the space-charge region of the junction predominates over the carrier diffusion mechanism, including the recombination and drift occurring in the bulk material, the devices are less efficient. Therefore, the use of HTM materials with lower offset levels and p-type perovskites with higher doping levels would be good alternatives for the organic compound spiro-OMeTAD in order to reduce the cost and increase the performance of the devices.

Funding

This work was partially supported by the National Council Research (CONICET), Argentina, by the Universidad Nacional Arturo Jauretche, Argentina, by the Universidad Nacional de Quilmes, Argentina, by the Universidad Nacional de La Plata, Argentina and by the Ministerio de Economía y Competitividad (Grant ENE2016-77798-C4-2-R), Spain.

References

- [1] M. Javad Taghavi, et al., Modeling of optical losses in perovskite solar cells, *Superlattice. Microst.* 97 (2016) 424–428.
- [2] F. Liu et al., Numerical simulation: toward the design of high-efficiency planar perovskite solar cells, *Appl. Phys. Lett.* 104 (2014) 253508 (4pp).
- [3] A. Baktash, et al., Improve efficiency of perovskite solar cells by using Magnesium doped ZnO and TiO₂ compact layers, *Superlattice. Microst.* 93 (2016) 128–137.
- [4] K. Adhikari, et al., Comparative study on MAPbI₃ based solar cells using different electron transporting materials, *Phys. Status Solidi C* (2015) 1–5.
- [5] M. Green, et al., The emergence of perovskite solar cells, *Nat. Photon.* 8 (2014) 506–514.
- [6] C. Zuo, et al., Advances in perovskite solar cells, *Adv. Sci.* 3 (2016) 1500324(16pp).
- [7] A. Kojima, et al., Organometal halide perovskites as visible-light sensitizers for photovoltaic cells, *J. Am. Chem. Soc.* 131 (2009) 6050–6051.
- [8] National Renewable Energy Laboratory (NREL), Efficiency chart, (April, 2018) <https://www.nrel.gov/pv/assets/images/efficiency-chart.png>.
- [9] J. Luo, et al., Water photolysis at 12.3% efficiency via perovskite photovoltaics and Earth-abundant catalysts, *Science* 345 (2014) 1593–1596.
- [10] G. Casas, et al., Analysis of the power conversion efficiency of perovskite solar cells with different materials as Hole-Transport Layer by numerical simulations,

- Superlattice. Microst. 107 (2017) 136–143.
- [11] M. Cappelletti, et al., Study of the electrical parameters degradation of GaAs sub-cells for triple junction space solar cells by computer simulation, Semicond. Sci. Technol. 31 (2016) 115020.
 - [12] S. Chatterjee, A. Pal, Introducing Cu₂O thin films as a Hole-Transport Layer in efficient planar perovskite solar cell structures, J. Phys. Chem. C 120 (2016) 1428–1437.
 - [13] R. Gottschalg, et al., The influence of the measurement environment on the accuracy of the extraction of physical parameters of solar cells, Meas. Sci. Technol. 10 (1999) 796–804.
 - [14] S. Yadir, et al., A new technique for extracting physical parameters of a solar cell model from the double exponential model (DECM), Opt. Mater. 36 (2014) 18–21.
 - [15] S. Sze, K. Ng, Physics of Semiconductor Devices, third ed., John Wiley & Sons, New Jersey, 2007.
 - [16] D. Chan, et al., A comparative study of extraction methods for solar cell model parameters, Solid State Electron. 29 (1986) 329–337.
 - [17] J.P. Charles, et al., Consistency of the double exponential model with physical mechanisms of conduction for a solar cell under illumination, J. Phys. Appl. Phys. 18 (1985) 2261–2268.
 - [18] M. Wolf, et al., Investigation of the double exponential in the current-voltage characteristics of silicon solar cells, IEEE Trans. Electron. Dev. 24 (1977) 419–428.
 - [19] J. Appelbaum, A. Peled, Parameters extraction of solar cells – a comparative examination of three methods, Sol. Energy Mater. Sol. Cells 122 (2014) 164–173.
 - [20] A. Zagrouba, et al., Identification of PV solar cells and modules parameters using the genetic algorithms: application to maximum power extraction, Sol. Energy 84 (2010) 860–866.
 - [21] J. Jervase, et al., Solar cell parameter extraction using genetic algorithms, Meas. Sci. Technol. 12 (2001) 1922–1925.
 - [22] M. Mitchell, An Introduction to Genetic Algorithms, Editorial MIT Press, 1999.
 - [23] M. Burgelman, et al., Modelling polycrystalline semiconductor solar cells, Thin Solid Films 361 (2000) 527–532.